Wafer-scale HfO2 encapsulated silicon nanowire field effect transistor for efficient label-free DNA hybridization detection in dry environment

Ganesh Jayakumar, Maxime Legallais, Per-Erik Hellstrom, Mireille Mouis, Isabelle Pignot-Paintrand, Valerie Stambouli-Sene, Céline Ternon, Mikael Östling

PAPER • **OPEN ACCESS**

Wafer-scale HfO_2 encapsulated silicon nanowire field effect transistor for efficient label-free DNA hybridization detection in dry environment

To cite this article: Ganesh Jayakumar *et al* 2019 *Nanotechnology* **30** 184002

OPEN ACCESS
IOP Publishing
Nanotechnology

Nanotechnology **30** (2019) 184002 (12pp)
https://doi.org/10.1088/1361-6528/aaffa5

Wafer-scale HfO_2 encapsulated silicon nanowire field effect transistor for efficient label-free DNA hybridization detection in dry environment

Ganesh Jayakumar[1,5,6], Maxime Legallais[2,3,5], Per-Erik Hellström[1], Mireille Mouis[3], Isabelle Pignot-Paintrand[2], Valérie Stambouli[2], Céline Ternon[2,4,6] and Mikael Östling[1]

[1] KTH Royal Institute of Technology, Department of Electronics, School of Electrical Engineering and Computer Science, Electrum 229, SE-164 40 Kista, Sweden
[2] Univ. Grenoble Alpes, LMGP, Grenoble, France and CNRS, LMGP, Grenoble, France
[3] Univ. Grenoble Alpes, IMEP-LaHC, Grenoble, France and CNRS, IMEP-LaHC, Grenoble, France
[4] Univ. Grenoble Alpes, LTM, Grenoble, France and CNRS, LTM, Grenoble, France

E-mail: ganeshj@kth.se and celine.ternon@grenoble-inp.fr

Received 12 September 2018, revised 6 December 2018
Accepted for publication 17 January 2019
Published 19 February 2019

Abatract

Silicon nanowire (SiNW) charge based biosensors are attractive for DNA sensing applications due to their compactness and large surface-to-volume ratio. Small feature size, low production cost, repeatability, high sensitivity and selectivity are some of the key requirements for biosensors. The most common e-beam manufacturing method employed to manufacture sub-nm SiNWs is both cost and time intensive. Therefore, we propose a highly reproducible CMOS industry grade low-cost process to fabricate SiNW-based field effect transistors on 4″-wafers. The 60 nm wide SiNWs reported in this paper are fabricated using the sidewall transfer lithography process which is a self-aligned-double-patterning I-line lithography process that also facilitates encapsulation of the SiNW surface with a thin HfO_2 layer on which DNA probes are grafted to finalize the biosensors. Upon DNA hybridization, SiNW devices exhibit threshold voltage shift larger than the noise introduced by the exposition to saline solutions used for the bioprocesses. More specifically, based on a statistical analysis, we demonstrate that 85% of the tested devices exhibit a positive threshold voltage shift after DNA hybridization. These promising results make way for the monolithic integration of SiNW biosensors and CMOS circuitry to realize a point of care device which can offer reliable real time electrical readout.

Keywords: silicon nanowire, DNA sensing, HfO_2 passivation, pattern transfer lithography, biosensor, silicon nanowire hybridization

(Some figures may appear in colour only in the online journal)

1. Introduction

In the past decade, assembly of one-dimensional structures such as SiNW, carbon nanotubes and nanonets have surfaced as favorable candidates for point of care (POC) label-free biosensing application [1–5]. In the field effect transistor (FET) configuration, these structures offer high sensitivity as

[5] Equally credited authors.
[6] Authors to whom any correspondence should be addressed.

their dimensions are comparable to the target biomarker of interest. SiNWs are particularly appealing due to their compatibility with microelectronics, compactness, potential for rapid electronic real time detection and mass fabrication [6–10].

In the literature, SiNW-FETs are notably manufactured using two major techniques—(1) bottom-up and (2) top-down [2, 11–14]. Vapor–liquid–solid is the most common bottom-up technique and allows for the growth of high volume of nanowires (NWs). However, it has been reported to cause tangling meshes, non-uniform line widths and manual errors when transferring to the substrate [3, 6]. On the contrary, the top-down technique relies on the established industry grade photolithography manufacturing process employed in the production of complementary metal-oxide-semiconductor (CMOS) electronic chips such as microprocessors, memory devices and smartphones etc. Since the top-down method is intended for large-scale mass production, the overall time and costs tend to be lower and is also best suited for the manufacturing of SiNW POC devices [11–13]. Besides, the NW fabrication technology and electrical properties, the quality of the dielectric encapsulating the NWs is also fundamental. First, the dielectric is the surface layer on which the biofunctionalization process is applied. As a consequence, in case of DNA hybridization detection, the surface termination should be able to covalently graft the DNA probes, therefore a high hydroxyl surface density is mandatory. Second, low leakage current and high dielectric constant will allow better sensitivity [15, 16]. Finally, it has been well established for pH sensing, that operation of SiNW in liquid environment causes charge screening and limits the sensitivity of the sensor to a maximum value of 60 mV pH^{-1}. This is termed as the Nernst limit of detection and is attributed to the formation of an electrical double layer (EDL) on the dielectric surface in the liquid environment [17]. Thus, the choice of the dielectric material should be such that it can withstand the maximum temperature during the manufacturing process, have consistent conformal deposition, low leakage current, defects and hysteresis and easy to transfer on the SiNW surface [15, 18] without obstructing the electrical access to the probing bond pads. Also, to attain high sensitivity of the sensors, insulators that have high density of OH groups and high dielectric constant are favored [18].

In this context, one of the best suitable candidate is HfO_2. Moreover, it is a well-established CMOS industry grade gate stack material, which is highly favorable to the top-down fabrication method. Yet, there are very few works that discuss wafer scale integration of HfO_2 with SiNWs for biosensing applications due to the clear lack of a cost and time efficient fabrication scheme.

With these constraints in mind, and in order to address the current lack of a reliable wafer-scale process without the use of complex or expensive technologies, we have developed a lithography process for manufacturing SiNWs. In this paper, we demonstrate a full CMOS compatible top-down self-aligned-double-patterning I-line lithography process called sidewall transfer lithography (STL) to fabricate 60 nm wide SiNWs on wafer scale using industry grade standard materials such as SiO_2, amorphous silicon (a-Si) and silicon nitride (SiN). The STL process that we have developed has the advantage of also facilitating the integration of HfO_2 on SiNWs and co-integration with CMOS circuits. In the following, after detailed explanation of the biosensing operating mechanisms, the SiNW-based bioFET fabrication scheme is presented. Then, the SiNW sensors are electrically characterized on 100 mm wafer scale and DNA sensing experiments are performed in dry environment. The dry environment DNA sensing experiments eliminates the issues of charge screening that may arise in the presence of a liquid but the sensing mechanism in dry state is still under debate and reproducibility has to be demonstrated. As a result, the sensors exhibit large threshold voltage shifts compared to previously reported values in literature [16, 19]. Thus, integration of HfO_2 with SiNW's can pave the way towards sophisticated sensitive, selective, and steady output POC sensors.

2. Biosensing operating mechanism

A SiNW-FET composes of four terminals—source, top gate, drain and back-gate. In our configuration shown in figure 1, three terminals—source, drain and back-gate—are electrically controlled by applying external potential while the top-gate is modulated either by the charges brought by the molecules bound to the dielectric surface or by the electrostatic coupling between the NWs and the molecules bound to the dielectric surface. For DNA hybridization detection operations, the NW-FET is first silanized (figure 1(1)) in view of functionalization with single strand DNA (figure 1(3)). After this step, the biosensor is ready for use and can be exposed to the target DNA which is complementary to the probe DNA (figure 1(4)). The driving force of such devices is not clearly understood and several mechanisms can be proposed alone or in competition. On the one hand, the electrostatic gating is linked to the charges brought at the surface by the molecules and that play the role of the top-gate which in turn impact the threshold voltage (V_{th}) of the FET as shown in figure 1. At each step, the shift in V_{th} is directly linked to the polarity of the molecules added on top of the SiNWs: a negative charge results in a positive shift, whereas a positive charge results in a negative shift. By monitoring the shift in the threshold voltage, the binding of molecules can be confirmed and the amount of charges present on the SiNW surface can also be estimated. On the other hand, electron doping from DNA to the nanostructured material is also proposed particularly when dealing with carbon-based materials [20].

In this work, in order to ensure that the different functionalization steps run smoothly and to study their impact on electrical properties, the FET transfer characteristics are measured at each step: after SiNW-FET manufacture (figure 1(1)), after silanization (figure 1(2)), after DNA grafting (figure 1(3)) and after DNA hybridization (figure 1(4)). At each step, a shift in threshold voltage is observed. However, for the biosensing operation,

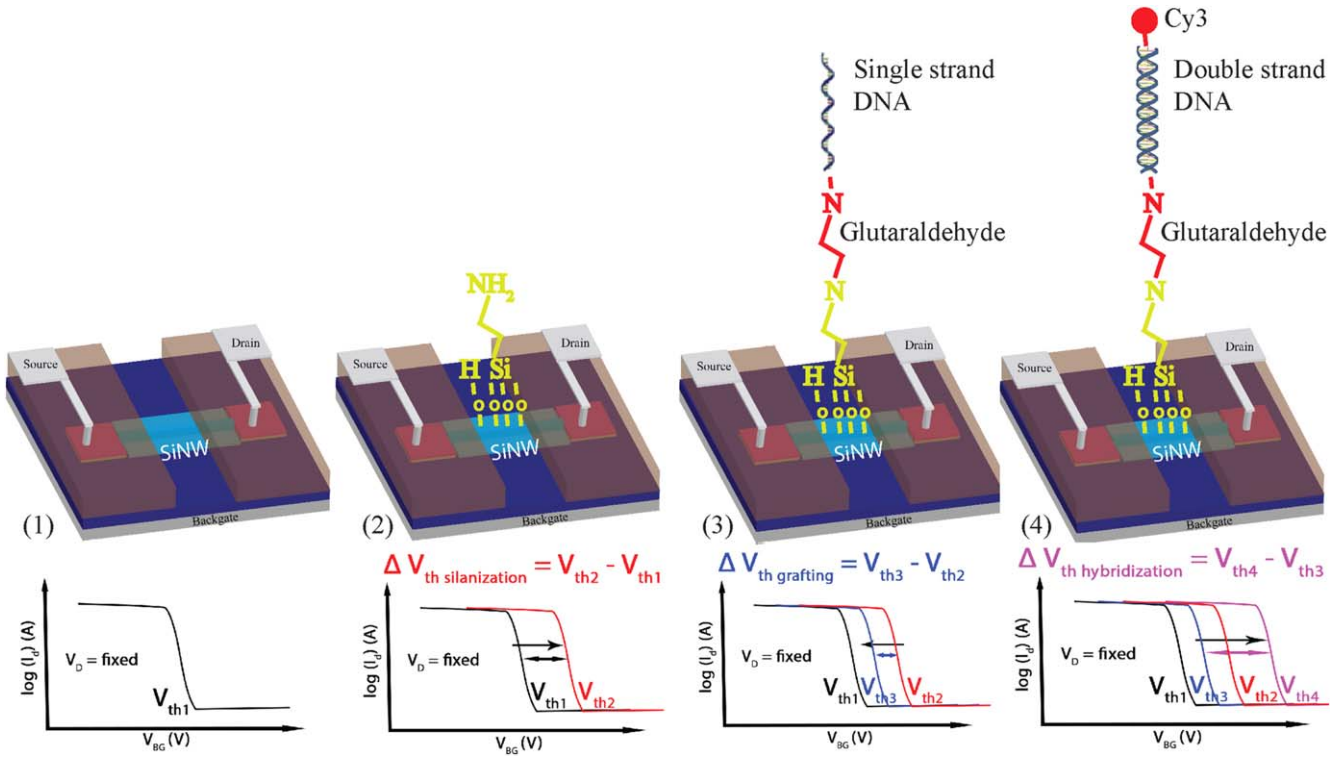

Figure 1. Schematic drawings illustrating the working mechanism of SiNW for charge based DNA detection. (1) A SiNW sensor prior to DNA functionalization. (2) The APTES surface modification on the SiNW (3) the DNA probe grafting and (4) the DNA hybridization with complementary Cy3-labeled target. By monitoring the change in threshold voltage after each step, the presence of DNA on top of SiNW can be detected.

only the last voltage shift ($\Delta V_{\text{th hybridization}} = V_{\text{th4}} - V_{\text{th3}}$) (figure 1(4)) is interesting.

To conclude, the SiNW sensing principle is based on the detection of changes in the environment around the SiNWs and particularly in the surface charge [15, 21]. The surface binding reactions occur on the thin dielectric material (1–10 nm) deposited on SiNW surface and that has to be properly chosen. Indeed, the DNA strand density directly depends on the silanization efficiency, which in turn depends on the specific amount of hydroxyl groups on the dielectric surface. Moreover, its dielectric constant and surface reactivity have been shown to influence the sensitivity of the sensor in liquid environment [17, 18, 22, 23].

Silicon by its nature forms a very stable oxide, SiO_2, that has very few dangling bonds and forms a formidable interface with the SiNW when fabricated at high temperature. Thus, research works have readily employed SiO_2 as the dielectric material. Using the SiNW in the ISFET [22] configuration (Ion Sensitive FET) with SiO_2 dielectric on top, numerous bio-, gas- and chemical-sensing studies have been performed to detect a range of targets such as pH, protein, DNA, metal ion, gas and humidity sensors [10, 11, 21, 23–25].

In spite of such varied applications, researchers have also recently reported poor performance of scaled SiO_2 dielectric based SiNW biosensor [15, 18]. This is attributed to persistent hysteresis and leakage currents [15, 18]. To overcome the above drawbacks of SiO_2 dielectric, high-k dielectric materials such as aluminum oxide (Al_2O_3) and hafnium oxide (HfO_2) are being explored [15, 18, 19, 26]. Al_2O_3 and HfO_2 have a high ionicity compared to SiO_2 [16, 18]. The ionicity is connected to the co-ordination number, which is related to the number of oxygen atoms surrounding the central Si, Hf or Al atom. In comparison to SiO_2 that has a co-ordination number of 4 and related ionicity of 0.45, Al_2O_3 and HfO_2 have co-ordination numbers of 6 and 8 and relatively high ionicities of 0.57 and 0.68 respectively [16, 18, 27]. Due to their high ionicity and hydroxyl groups on the surface, high pH response has been shown to arise from sensors employing Al_2O_3 and HfO_2 [16, 17, 19]. However, despite its high dielectric constant, Al_2O_3 has also been reported to cause very similar issues as seen on thin SiO_2 films such as poor interface and hysteresis [15]. Instead, HfO_2 is very attractive and has been reported to have surplus OH groups on its surface [18, 19, 26, 28, 29]. Recent works have demonstrated sensitivity values close to the Nernst limit of detection by employing HfO_2 as sensing dielectric in FinFET based sensor configurations operated in liquid environment [16]. However, wafer scale integration of HfO_2 with SiNWs lacks of efficient fabrication scheme. In the next part, we expose our highly efficient and innovative CMOS industry grade low cost process to fabricate SiNWs encapsulated with a thin layer of 4.5 nm HfO_2 at the wafer scale.

3. BioFET fabrication

The bio-FET fabrication is composed of two main steps: the SiNW FET fabrication and the biofunctionalization. For the

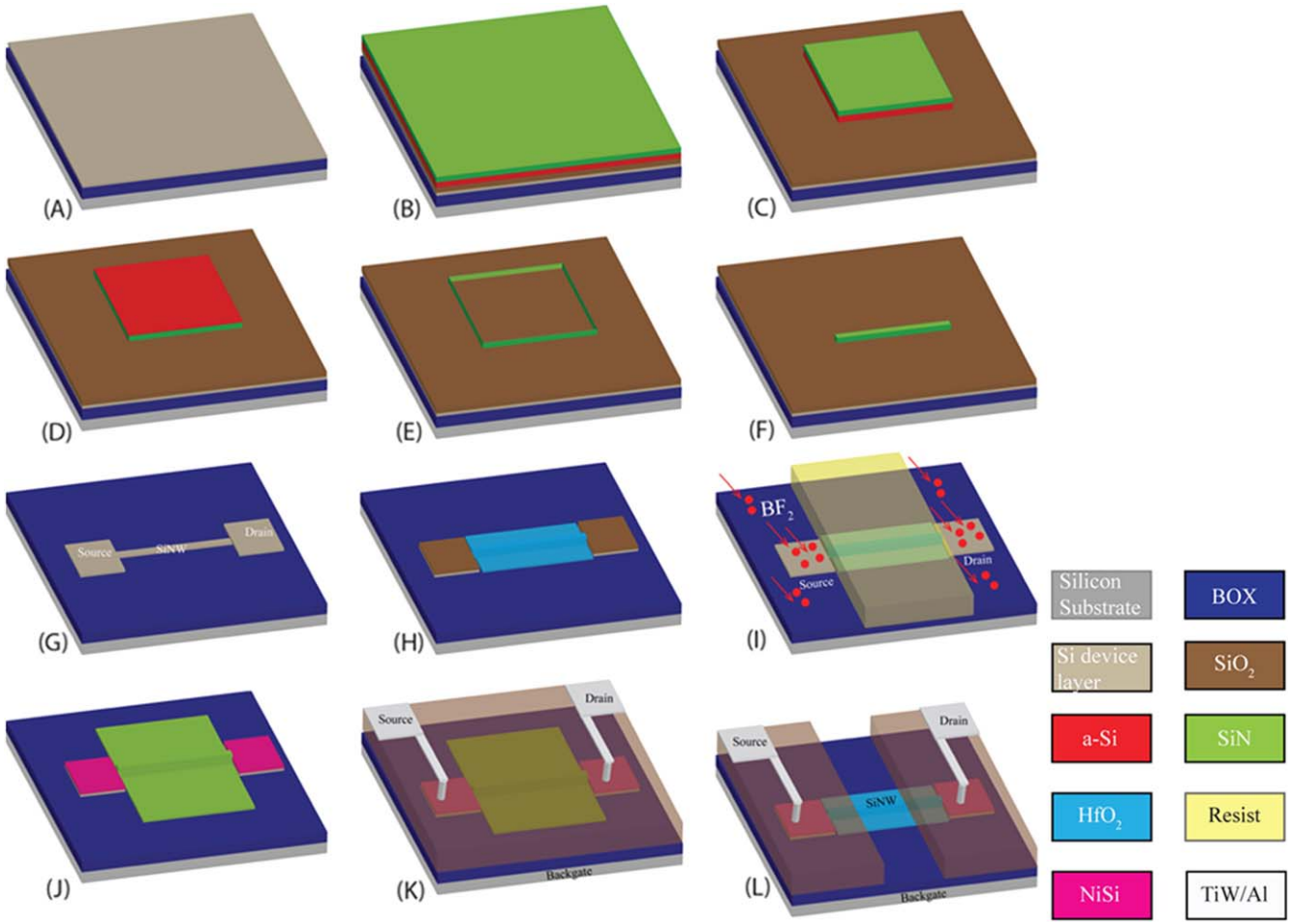

Figure 2. Schematic of top-down fabrication steps used to manufacture a SiNW sensor (A) Starting substrate is silicon on insulator (SOI) wafer. The c-Si device layer is thinned from 55 to 20 nm by thermal oxidation. (B) Then a tri-layer stack of SiO_2 (40 nm), a-Si (100 nm) and SiN (40 nm) is deposited (C) a-Si is selectively etched using SiN as mask to form vertical sidewalls (D) 60 nm SiN spacer is deposited and etched to form spacers (E) a-Si is selectively etched using TMAH to leave only SiN spacers on SiO_2. (F) One of the spacer is selectively removed using diluted HF and resist mask. (G) Source/drain contact pads and SiNW pattern is defined in c-Si device layer using SiO_2/SiN mask. (H) Pedestal SiO_2 (4.5 nm) is grown on top of SiNW, ALD HfO_2 (4.5 nm) is deposited and etched using resist mask. The SiO_2 layer behaves as etch stop during the HfO_2 etch. (I) BF_2 ion-implantation of source/drain regions is performed using resist mask. (J) NiSi ohmic contacts are formed using salicide process. (K) Contact holes are etched in the SiO_2 inter-layer dielectric and TiW/Al metal pads are defined. (L) Using a resist mask and RIE, the inter-layer dielectric lying on-top of SiNW is etched.

FET fabrication, we develop a highly efficient 4″-wafer-scale HfO_2 encapsulated SiNW FET integration process. Then, for the first time, we successfully apply our biofunctionalization process to the HfO_2 passivated SiNWs in dry environment and demonstrate reproducible efficient DNA hybridization detection.

3.1. Wafer-scale SiNW FET integration process

Figure 2 shows the steps involved in the fabrication of the SiNW sensor using the STL process in the fully depleted silicon on insulator technology. In this article, only the salient steps that is relevant for high-K integration during SiNW fabrication is presented. The other challenges and details of co-integration of SiNWs with CMOS using the STL process are described elsewhere [12, 13].

3.1.1. SOI wafer thinning and back-gate formation (figures 2(A) and (B)). The starting substrate is the p-type ($\rho =$ 14–19 Ω cm) SOI wafer with crystalline silicon (c-Si) thickness of 55 nm and buried oxide (BOX) layer thickness of 145 nm. Thermal oxidation was performed to thin the c-Si device layer to 20 nm (figure 2(A)). The grown 70 nm thermal oxide was thinned down to 30 nm using RIE.

3.1.2. SiNW definition using STL (figures 2 (B)–(E)). Later, deposition of a bi-layer stack of a-Si sidewall sacrificial layer and SiN followed (figure 2(B)). After I-line photolithography, the SiN is dry etched in Applied Materials P5000 cluster tool using CHF_3/CF_4 chemistry. The resist is stripped in H_2SO_4: H_2O_2 [3:1]. The SiN serves as a hard mask for etching a-Si by RIE using Cl_2/HBr chemistry (figure 2(C)). The SiN hard mask is then stripped in H_3PO_4. In the next step, a thin film of SiN called SiN spacer is deposited on the entire wafer surface

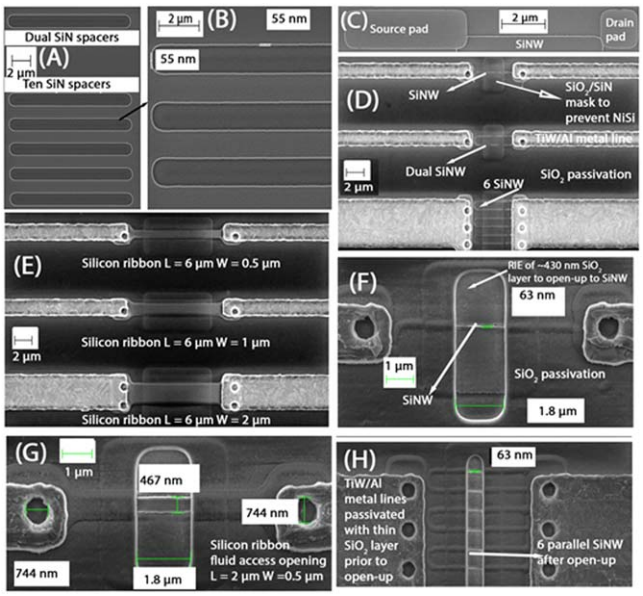

Figure 3. (A) Top-view SEM image after SiN spacer formation corresponding to figure 2(E) of the fabrication step. (B) Close-up image of an array of ten SiN spacers of line width ~55 nm lying on top of the SiO_2 hard mask. (C) Top-view SEM image of single SiNW lying on-top of the BOX with well-defined source/drain pads. This step corresponds to steps of figure 2(F) is final step in the STL process. It also indicates the wet-etch step that was performed to remove one of the SiN spacers and RIE of the SiO_2 hard mask. (D)–(E) Top view SEM images of single, double, array of six NWs, silicon ribbons of fixed length (6 μm) and varying width (0.5, 1, 2 μm) prior to opening tracks to access the SiNW's. These steps correspond to steps of figure 2(K). (F)–(H) Top view SEM images of single nanowire, silicon ribbon ($L = 2$ μm and $W = 0.5$ μm) and array of six nanowires after opening access to the SiNW test site. These steps correspond to steps of figure 2(L). The image also shows the passivation of metal lines with thin SiO_2 dielectric layer.

using the P5000 cluster tool and etched back to form sidewall spacers without breaking vacuum (figure 2(D)). The line width of the SiNW is controlled by the thickness of the SiN spacer. In this case, 60 nm SiN spacer was deposited. This is followed by wet etch of a-Si in tetra-methyl-ammonium-hydroxide (TMAH) (figure 2(E)) which yields SiN spacers lying on top of the SiO_2 hard mask (figures 2(D) and (E), figures 3(A) and (B)).

3.1.3. Active area definition—optional (figure 2(F)). Next, a lithography step and a very short wet etch in 1% HF solution is used to define the pattern where one of the SiN spacers is targeted to be removed. This step is essential to form single SiNW while is non-essential in the case of array of double or six SiNWs (figure 2(F)).

3.1.4. Contact pad formation (figure 2(G)). Utilizing photolithography, a resist mask is patterned on top of the devices to define source and drain contact pads, then the underlying oxide hard mask is subsequently etched with very good selectivity of 6:1 to the SiN spacers using CHF_3 RIE process. Lastly, after stripping of the resist, the c-Si device layer is etched in Cl_2/HBr to form 20 nm × 60 nm SiNWs (thickness × width) and the source and drain pads (figures 2(G) and 3(C)). After patterning of the c-Si device layer, the SiO_2 and SiN hard masks are stripped using 5% HF solution. This step recesses the BOX layer to ≈90–95 nm.

3.1.5. Dielectric integration on SiNWs (figure 2(H)). As it is very well established that the direct deposition of HfO_2 on Si forms poor interface and threatens the electrical performance, a thermal oxidation step is performed to ensure a good interface to the SiNW [30, 31]. Hence, a thin 4 nm pedestal SiO_2 is grown on top of the SiNW by oxidizing in O_2 at 800 °C before the HfO_2 deposition. This was followed by the atomic layer deposition (ALD) of 4.5 nm HfO_2 on top of the SiO_2 at 350 °C using HfD-04 and DI water as precursors. In the next step, a resist mask is used to selectively remove the HfO_2 on the source/drain pads of the SiNW using plasma etching in BCl_3/Cl_2 chemistry (figure 2(H)). Pertaining to this step, since the Cl_2 can attack the underlying c-Si, the pedestal SiO_2 also serves as an etch stop for the HfO_2 etch and in the process avoids the damage of the c-Si device layer.

3.1.6. Source/drain formation using ion implantation process (figure 2(I)). In the next step, employing a resist mask, 13 keV energy, 7° tilt angle (to avoid channeling) and a dose of 10^{15} cm^{-3}, the source/drain regions were ion-implanted with the BF_2 species (figure 2(I)). After stripping the resist mask in O_2 plasma, the dopants were activated at 1000 °C by performing rapid thermal annealing (RTA) for 10 s.

3.1.7. Contact formation using the salicide process (figure 2(J)). In this step, low resistance NiSi ohmic contacts are formed by using the salicide process (figure 2(J)). Since the salicide process forms self-aligned contacts, it is undesirable to have NiSi formation on top of the SiNW as it will lead to electrical shorting of source and drain regions. Therefore, a SiO_2 (10 nm)/SiN (20 nm) dielectric stack is deposited on top of the devices and a resist mask is used to etch the SiO_2 and SiN on top of the source/drain regions while preserving it on top of the SiNW (figures 3(D) and (E)). Then, a short 1% HF spray clean was performed to remove the native oxide and 10 nm Nickel was deposited on the wafer using Applied materials Endura physical vapor deposition (PVD) tool. A RTA at 450 °C for 30 s followed to form NiSi. Then the unreacted Ni was selectively removed by wet etching for 10 min using the piranha mixture.

3.1.8. Via formation and metal deposition (figure 2(K)). A 400 nm thick PECVD SiO_2 inter-layer dielectric (ILD) was deposited and a lithography step was employed to define contact holes. Then a standard 100 nm TiW lining layer and 500 nm Al metal layer was deposited using PVD and patterned (figures 2(K), 3(D) and (E)).

3.1.9. Passivation and open-up to SiNW (figure 2(L)). In this step, tracks were defined to access the SiNW using a lithography mask and a combination of dry etch in CHF_3/CF_4 chemistry (to etch the stack of SiO_2/SiN) and short diluted

Table 1. Name and geometrical characteristics of studied devices. The width of the nanowires (NW) is 60 nm. The thickness of NWs and nanoribbons (NRs) is 20 nm. '$N = X$' means 'X NWs in parallel' and W refers to NR width.

		$L = 6\ \mu$m	$L = 2\ \mu$m	$L = 1\ \mu$m
NW	$N = 1$	A	G	M
	$N = 2$	B	H	N
	$N = 6$	C	I	O
NR	$W = 0.5\ \mu$m	D	J	P
	$W = 1\ \mu$m	E	K	Q
	$W = 2\ \mu$m	F	L	R

wet etch in 1% HF solution ((figures 2(L), 3 (F)–(H)). It is worth noting that this simple approach to access the SiNW avoids the usage of complex microfluidic channels. In the final step, a forming gas (20:1 N_2/H_2) anneal is performed at 400 °C.

Apart from SiNWs (single NW, array of double NWs and six NWs), reference structures, manufactured using traditional I-line lithography that had substantially wider dimensions were also included. For the remainder of the document these structures will be addressed as silicon ribbons. The final dimensions of the SiNW structures are 6–2–1 μm × 60 nm × 20 nm (length × width × thickness) while the number of parallel SiNWs varies from 1 to 6. The ribbons had same length (6–2–1 μm) and thickness (20 nm) and varying widths (0.5–1–2 μm) respectively. Table 1 summarizes the geometrical characteristics of the fabricated devices. In conclusion, the integration process detailed here allows the simultaneous manufacture of 18 devices per 7 × 7 mm^2 chip, each 4″ wafer containing 108 chips, i.e. a total of 1944 devices including 9 SiNW-based FETs at wafer scale.

3.2. Biofunctionalization

Operation as a biosensor is obtained by means of two steps. In the first step, the probe molecules are immobilized on the active part of the device and this is part of the biosensor fabrication process. In the second step, the sensor is put in contact with the analyte that potentially contains the target molecules to be detected. For this research study, we used model molecules and buffers as well as lab processes, which would later have to be adapted and co-developed with the microfluidic packaging environment.

3.2.1. Biofunctionalization for biosensor finalization. The DNA probe immobilization on the devices, called DNA grafting, was realized through a multistep functionalization procedure applied to the HfO_2 deposited on top of NWs and ribbons.

The first step (figure 1(2)) consisted of covalent grafting of an aminosilane to the surface. To this aim, air plasma was applied to the chip so that it turned the HfO_2 surface into hydroxyl groups. Then, the highly reactive surface was exposed to the APTES (aminopropyltriethoxysilane). For this work, we chose the vapor phase process in anhydrous conditions (under nitrogen gas environment) described by Serre *et al* [1]. Briefly, the hydroxylated chip was placed in a chamber containing 150 μl of APTES sealed under a low humidity atmosphere (1% relative humidity). The chamber was placed in a furnace at 80 °C for 1 h so that the condensation reaction occurred between the –OH surface termination groups and the silanol APTES groups. Then, the chip was rinsed with dry ethanol and annealed at 110 °C for 1 h.

For the second step (figure 1(3)) which leads to the covalent grafting of single strand DNA probes, the chip was first immersed in a 2.5% glutaraldehyde ($CHO–(CH_2)_3–CHO$) water solution at room temperature for 90 min so that molecules of glutaraldehyde were covalently linked to the APTES functionalized surface. Then the immobilization of single strand (ss)-DNA probes (5′-NH_2-TTTTT GAT AAA CCC ACT CTA-3′) was achieved by depositing a droplet (1 μl) of the DNA probes (10 μM) diluted in a sodium phosphate solution (0.3 M) at the surface of the functionalized samples and drying overnight. Finally, DNA probe stabilization was done using a 0.1 M sodium borohydride ($NaBH_4$) solution.

3.2.2. Biodetection. The biodetection is based on the highly efficient and selective DNA hybridization. In this study, our aim is to demonstrate that the dry-state DNA hybridization detection is a real opportunity for SiNWs. As a consequence, this work is focused on studying statistically the electrical changes upon DNA hybridization rather than on studying the biosensor performances (selectivity and sensitivity). Therefore, we concentrated the experimental work on a single complementary DNA concentration compared to the biosensor exposed only to the buffer solution to exclude the contribution of salt to the observed phenomenon.

For hybridization (figure 1(4)), first a solution of DNA targets at a concentration of 2 μM was prepared in a buffer solution (pH = 7) which contained a phosphate buffered saline tablet and a sodium chloride powder diluted in deionized water. 2 μl of this solution was deposited on the active area of the chips and then the samples were incubated for 45 min in a humid chamber at 42 °C. Finally, an intensive rinsing was performed to remove any residuals from the buffer solution and the chips are dried. The complementary DNA targets labeled with a cyanine (Cy3) fluorescent dye (3′-AC CTA TTT GGG TGA GAT AC-Cy3-5′) was employed for the hybridization. Labeling with fluorescent dyes is not required for the operation of this type of sensor which is based on electrical detection. Nonetheless, it was used here to perform optical verification of the efficiency of DNA grafting and hybridization process: hybridization allows fluorophore immobilization on the surface along with fluorescence signature.

Electrical properties in the transistor configuration were measured in dry environment. Working in dry environment allows circumventing the difficulties linked to the screening of the DNA charges by the positively charged counter-ions

present in the electrolyte. Indeed, such screening directly impacts the reliability, making results dependent on the characteristics of the electrolyte medium. Furthermore, on account of the charge redistribution within the EDL, the sensitivity of the biosensor is also reduced as the surface potential shift is too weak to be detected [32–34]. When the detection is carried out in dry state, according to the literature, several mechanisms can occur alone or in competition [20, 35, 36]. For SiNWs, we suppose that the dominant mechanism is linked to the electrostatic gating. For example, after ion rinsing, the negative charge of the DNA target molecules is then balanced by changes in the concentration of free carriers in the NWs instead of being balanced by electrolyte counter-ions [32]. In order to confirm this hypothesis, a statistical study was carried out to follow the characteristics of the transistors before any functionalization, figure 1(1) and after each main step (further called biochemical steps), silanization figure 1(2), ss-DNA grafting figure 1(3) and hybridization, figure 1(4). For the last step (hybridization), a systematic comparison with a reference biosensor exposed only to the hybridization buffer, free of complementary-DNA, was conducted.

4. Methods

4.1. DNA grafting and hybridization detection

APTES, (3-Aminopropyl)-triethoxysilane, was bought from Carl Roth and glutaraldehyde 10%, was bought from Sigma–Aldrich. Single strand DNA (ssDNA) was synthesized by Biomers. The sensor was designed for the detection of ssDNA target hybridization with complementary ssDNA probes grafted on the sensor. The target was labeled with a cyanine (Cy3) fluorophore, and DNA hybridization was confirmed by fluorescence measurements. The DNA probes were diluted at 10 μM in a sodium phosphate solution (0.3 M, pH 9) and the target DNA sequences were diluted at 2 μM in a hybridization solution composed of phosphate buffered saline 0.1 M and NaCl 0.5 M, in deionized water (pH 7).

4.2. Electrical characterization

For full-scale wafer mapping, a Cascade 12000 semi-automatic wafer prober that was externally connected to a Keithley 4200-SCS parameter analyzer was used to perform DC electrical measurements. The electrical measurements were performed by applying a back-gate voltage (V_{BG}) to the substrate from the front pad and sweeping from values of -5 to $+5$ V. The drain terminal (V_D) was biased with a value of -0.1 V while the source terminal (V_S) was connected to ground. For electrical monitoring of functionalization and biosensing efficiency, at the chip level, three-terminal configuration, I_D–V_D–V_{BG}, measurements were performed at room temperature, in the dark using a Karl Süss probe station controlled by a HP 4155 parameter analyzer. The back-gate voltage (V_{BG}) was applied directly to the back-side of the substrate via the sample holder, sweeping from values of $+10$ to -5 V.

4.3. Optical characterization

Fluorescence measurements were performed in different modes after each hybridization procedure in order to evaluate the hybridization rate. First an Olympus BX41M epi-fluorescence microscope coupled with a 100 W mercury lamp was used. Cy3 dyes were excited at 550 nm and emitted fluorescence recorded at 570 nm. Second, fluorescence measurements were performed with a confocal laser scanning microscope Zeiss LSM700 equipped with a 63× oil objective (numerical aperture 1.4). For emission wavelength we use the 555 nm diode laser line and for the detection of the emitted fluorescent light, the MBS405 (main dichroic beam splitter) is used and the detection window adjusted with the VSD (variable secondary dichroic) from 560 to 700 nm. All images were collected with pinhole set at 1 Airy Unit. The Image Pro plus software was used for image analysis and to determine the fluorescence intensity inside the regions of interest.

5. Results and discussion

5.1. Electrical characterization of as-fabricated FETs

Figure 1(1) shows the electrical setup used to measure the SiNW electrical properties after fabrication. The silicon NWs and ribbons were measured on wafer scale (figure 4). From the transfer characteristics (I_D–V_{BG} curves) of the different test structures it is evident that the SiNWs and ribbons behave as MOSFETs (figure 4). In the back-gate voltage (V_{BG}) range from 5 to 2 V, the devices are in off-state and drain current, I_D, is $\leqslant 1$ pA while in the voltage range $-5 \leqslant V_{BG} \leqslant 0$ V, the devices are in the on-state and I_D is $\geqslant 10$ nA. The measured I_{on}/I_{off} ratio is above 10^5. The devices exhibit well-behaved subthreshold characteristics with subthreshold slopes around ≈70–75 mV/dec indicating an interface state density of $4 \times 10^{10}\,cm^{-2}\,eV^{-1}$ at the c-Si/BOX interface. The threshold voltage was extracted by linear extrapolation method and the measured range of the threshold voltage was less than 2 V for the devices (see figure 4). This spread is speculated to be predominantly from variations in the amount of fixed charges at the c-Si/BOX interface since the subthreshold slope was found not to depend on the measured threshold voltage. Furthermore, a relatively modest change of fixed charges of $3 \times 10^{11}\,cm^{-2}$ would induce a threshold voltage shift of 2 V due to the BOX thickness of 145 nm. The threshold voltage variation between devices can effectively be reduced by employing a thinner BOX layer.

5.2. Evaluation of biofunctionalization effectiveness

The DNA immobilization procedure described in previous section was applied to the set of devices described in table 1. To confirm that the hybridization procedure was successfully conducted, and that DNA was well grafted and hybridized on the SiNWs and ribbons, the fluorescence signal was

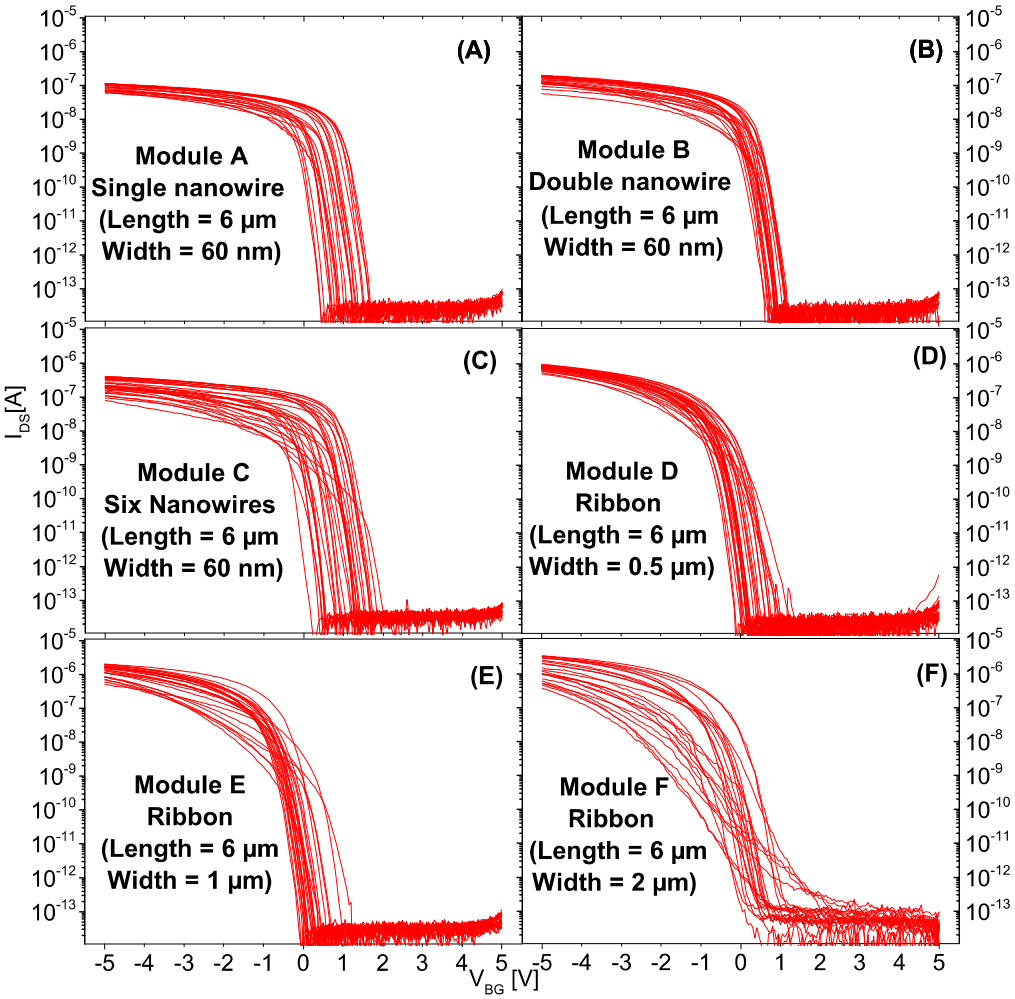

Figure 4. I_D–V_{BG} curves of different test structures with thin pedestal (4.5 nm) thermal SiO_2/HfO_2 (4.5 nm) on-top. (A) Single nanowire $L = 6\ \mu$m, $H = 20$ nm, $W = 60$ nm. (B) Double nanowire $L = 6\ \mu$m, $H = 20$ nm, $W = 60$ nm. (C) Six nanowires $L = 6\ \mu$m, $H = 20$ nm, $W = 60$ nm. (D) Silicon ribbon $L = 6\ \mu$m, $H = 20$ nm, $W = 0.5\ \mu$m. (E) Silicon ribbon $L = 6\ \mu$m, $H = 20$ nm, $W = 1\ \mu$m. (F) Silicon ribbon $L = 6\ \mu$m, $H = 20$ nm, $W = 2\ \mu$m. For each test structure, 108 different devices were characterized.

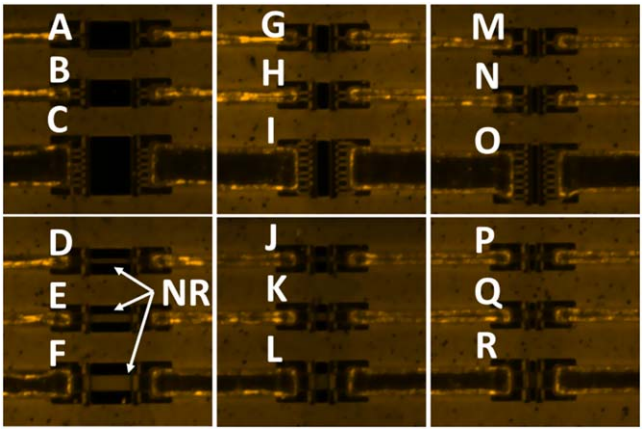

Figure 5. Fluorescent images captured with a confocal laser-scanning microscope of devices after the DNA hybridization with a complementary Cy3-labeled DNA target. Device properties are detailed in table 1.

measured. Due to the poor spatial resolution of standard fluorescence microscope, the small dimensions of the studied devices required the use of a confocal fluorescence microscope with better spatial resolution (figure 5). The fluorescence signal observed on all nanoribbon-based devices (NR) clearly confirms that the DNA hybridization, and hence grafting, did successfully occur. The silanization (figure 1(2)), grafting (figure 1(3)) and hybridization (figure 1(4)) procedure was thus confirmed. However, even with such a powerful tool, the magnification was insufficient to observe the fluorescence of the NWs (devices A–C, G–I and M–O).

The normalized intensity of fluorescence of the largest NRs (F, L and R) changed from 0.80 for F to 0.60 for L and finally 0.38 for R when the length of the channel decreased from 6 to 2 μm and 1 μm. This tends to show that the degree of grafting and/or hybridization depends on channel length, with reduced efficiency at shorter lengths. Such a behavior was attributed to the variation in geometry, with reduced

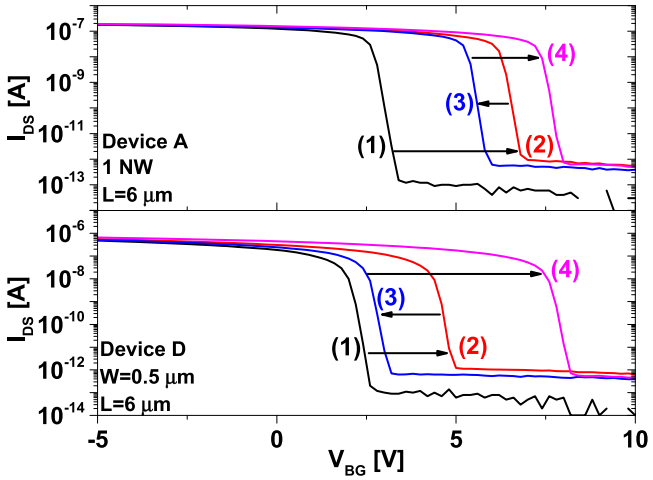

Figure 6. Electrical properties of Si nanowire (top) and ribbon (bottom) based device (type A and D, table 1). I_D–V_{BG} curves at $V_D = 0.1$ V before any functionalization (step 1, black) and after silanization (step 2, red), after DNA grafting (step 3, blue) and after hybridization (step 4, pink).

access to NWs surface for shorter channels. Indeed, as explained in the previous part, the devices were encapsulated with a 400 nm SiO_2 layer, in which a window was opened above the nanostructures to allow localized biofunctionalization (figures 1 and 2(L)). The size of this window decreased with channel length reaching dimensions ($1-2$ μm) for which surface tensions can impede the penetration of liquids to the bottom of the cavities, reduce the effectiveness of grafting and hybridization processes, and thus result in lower fluorescence intensity. These first observations suggest that a minimum channel length is required for biosensor applications.

5.3. Label-Free DNA hybridization detection

5.3.1. Electrical evaluation of the bio FET. The electrical properties of the devices were investigated before any functionalization (figure 1(1)) and after silanization (figure 1(2)), probe grafting (figure 1(3)) and hybridization (figure 1(4)). Apart from measuring the transfer characteristics (I_D–V_{BG} curves), the threshold voltage (V_{th}) was extracted as it gives direct information about charge changes at the channel surface. Before studying in details, the effect of hybridization on the transistor characteristics, a reference biosensor (figure 1(3)) was submitted to the hybridization buffer, free of complementary-DNA. The aim of this experiment is to determine the impact of FET exposure to saline solutions by monitoring the electrical properties of the FET. This will ensure that the measured changes in biodetection experiments have their origin in the hybridization and not in salt crystallization on the surface after drying. So, the treatment introduced some variability on the I_D–V_{BG} curves (not shown here). However, the threshold voltage was impacted by less than 0.2 V. Thus, $|V_{th}|$ shifts larger than 0.2 V in biodetection experiments can be considered as significant charge variation at the surface of the channel.

Figure 6 gives typical I_D–V_{BG} curves for a NW (device A) and NR (device D) transistor after each biochemical step. As expected, the transfer characteristics were translated, with a shift in threshold voltage, while subthreshold slope and I_{on}/I_{off} ratio remained almost constant. Such similar behavior confirms that field-effect electrostatic coupling occurs between surface charged molecules and the transistor channel. A V_{th} shift towards positive voltages (right shift) results from the presence of negative charges at the surface, whereas a shift towards negative voltages (left shift) is associated with positive charges. According to figure 6, a right shift was observed after silanization. It was attributed to the presence of oxygen negative charges on the top of the SiNW channel. The DNA grafting resulted in negative ΔV_{th}, which is a signature for the addition of a positive charge. This result seems surprising because addition of DNA, which is negatively charged, should result in a positive shift. However, one should keep in mind that this step accounts for addition of glutaraldehyde and single strand DNAs on top of the device. Furthermore, it has been previously demonstrated that glutaraldehyde grafting on SiNWs induced an important negative shift, larger than the subsequent positive shift induced by the DNA grafting [37], thus explaining the observed negative shift of threshold voltage. Finally, the hybridization, which consists in adding complementary single strand DNAs that match perfectly the probe DNAs grafted on the surface, was followed by an increase in the threshold voltage (positive ΔV_{th}), which is a signature for the addition of a globally negative surface charge. It should be noted that in their study dealing with single SiNW transistors, Chu *et al* observed exactly the same alternation of right and left shift for the same steps [37]. These first observations tend to confirm that the charges of the molecules are not counterbalanced by counterions but do imply a change in the distribution of charges within the nanostructures.

As a conclusion, from figure 6, it can be deduced that hybridization between target and probe, which is the important step from application point of view, could be safely detected from the associated threshold voltage shift.

5.3.2. Impact of geometry on biosensing. Each device, from A to F, was electrically characterized and clear tendencies were obtained, as shown in figure 7, which gives the evolution of the threshold voltage after each biochemical step (from 1 to 4). First, a relatively large dispersion was observed in V_{th} value after the silanization step (step 2), from 2 to 6.5 V, with no particular correlation with device geometry. Then, regarding the effect of DNA grafting (step 3) and DNA hybridization (step 4), all devices behaved similarly, even if the absolute value was, once again, widely dispersed.

Figure 8 displays the biodetection efficiency as a function of transistor geometry (length, width, NWs, NRs). Biodetection efficiency was defined as the ΔV_{th} shift after hybridization (between the steps 3 and 4 in figure 1).

From figure 8, the clear tendency observed in figure 7 was again confirmed for the longest devices, resulting in a positive ΔV_{th}. However, for short devices, very low or no

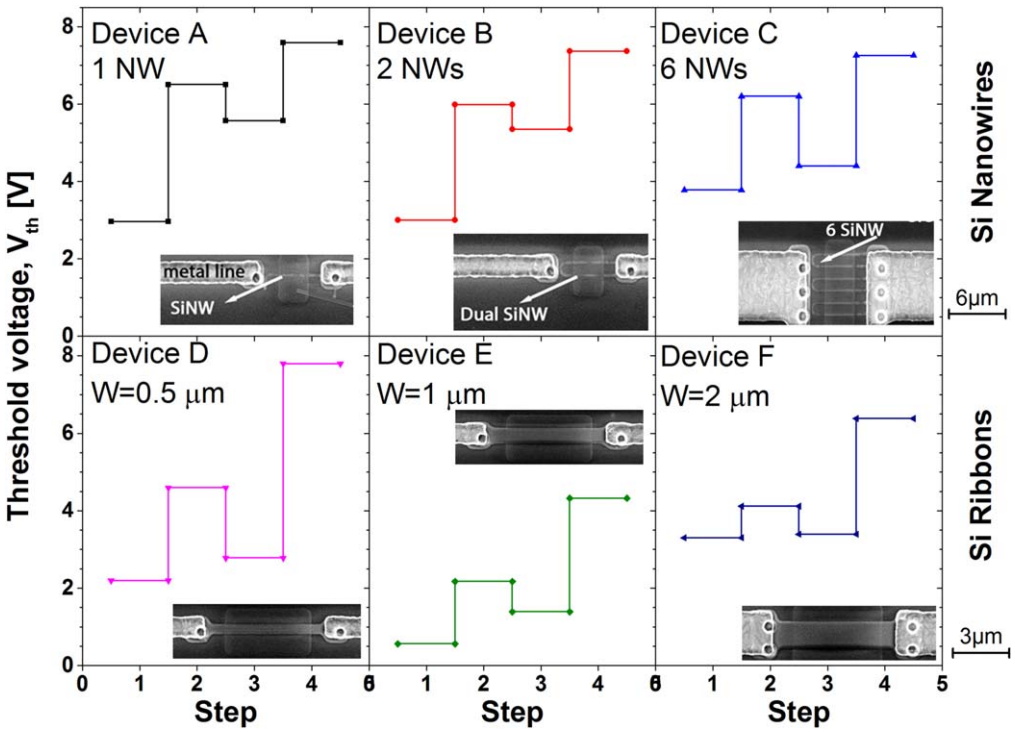

Figure 7. Threshold voltage value after each biochemical reaction step for various devices. Step 1: before any functionalization; step 2: after silanization; step 3: after grafting; step 4: after hybridization. For each device, the SEM image is displayed. Top and bottom scale bars are respectively associated to SEM image for NWs and ribbons.

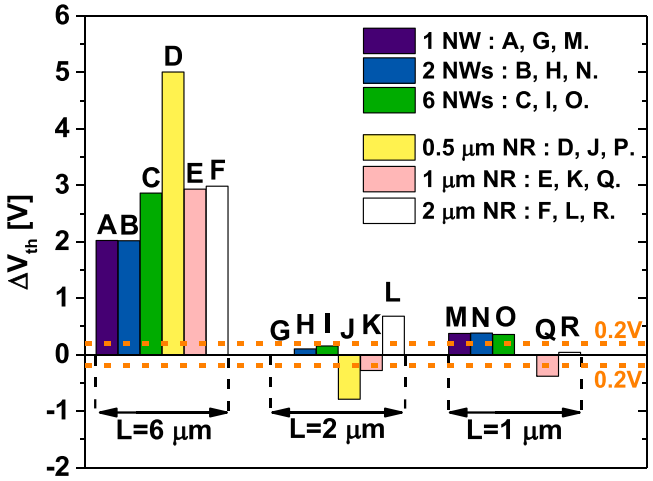

Figure 8. Shift in threshold voltage between hybridization and DNA grafting of all transistors of one chip. Devices are classified according to their length.

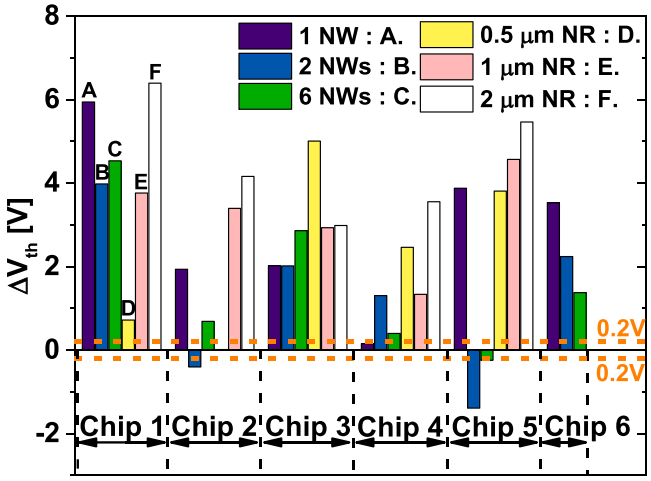

Figure 9. Shift in threshold voltage between hybridization and DNA grafting of 33 transistors spread over six chips. Device channel length is 6 μm.

significant V_{th} shift was observed. This observation was found consistent with the reduction in the degree of grafting and hybridization at short channel length that had been already suspected from confocal microscopy observations (figure 5) and would confirm that the windows giving access to the NWs and NRs are too tiny to allow efficient DNA grafting and/or hybridization in these devices.

As a result, the longest devices, with 6 μm length active area, were found to be the best suited for DNA biosensing and were analyzed in more details.

5.3.3. Statistical study of biosensing. A variability study was conducted on the 6 μm channel length biosensors. For this purpose, six chips were used, each of them containing 18 different transistors (devices A–R table 1) among which six devices are well designed for the biosensing (devices A–F table 1). A total of 33 biosensors were effectively operational, out of the 36 biosensors theoretically available. Their detection efficiency is displayed in figure 9.

Among them, 28 transistors (85%) exhibited a positive ΔV_{th} shift after hybridization; two gave rise to a non-significant

shift ($|Vth|<0.2$ V) and three to a negative shift, which is in contradiction with the expected behavior, suggesting defective devices.

Moreover, neither the decrease in active surface area, nor the increase in number of parallel NWs seemed to be of interest for better hybridization detection. Indeed, apart from the length-related effect mentioned above, no clear tendency linked to the geometrical parameters was observed in figure 9, resulting in an average value of 2.4 V for the V_{th} shift. The variability observed between identical samples in the shift value could be attributed to the influence of salt concentration variations on account of liquid being taken away on the DNA binding. Indeed, DNA hybridization relies on equilibrium and is a dynamic process which could be influenced by experimental conditions of rinsing or drying. However, the reproducibility of the positive shift upon hybridization confirms that the DNA hybridization detection in dry environment is highly reliable process as long as the positive shift in threshold voltage is used to assess the detection.

5.3.4. DNA grafting evaluation. Finally, the quantity of immobilized charges on the surface of the nanostructures was estimated from the mean threshold voltage shift. Indeed, the surface density of additional charges immobilized during hybridization (N_{hybrid}) is deduced from the surface density of charges (Q_{hybrid}), which is directly linked to the threshold voltage shift by the following relationship: [38]

$$N_{hybrid} = \frac{Q_{hybrid}}{q} = -\Delta V_{th}\frac{\varepsilon_0\varepsilon_r}{qt_{ox}}, \quad (1)$$

where ε_0 is the vacuum permittivity ($\varepsilon_0 = 8.85 \times 10^{-14}$ F cm^{-1}), ε_r the relative permittivity of the gate dielectric ($\varepsilon_r = 3.9$ for SiO_2) and t_{ox} its thickness (90 nm). q is the charge of electron ($q = -1.6 \times 10^{-19}$ C). The surface density of negative charges immobilized during hybridization that can be deduced from the average threshold voltage shift of 2.4 V is thus of the order of $N_{hybrid} = 3.6 \times 10^{11}$ cm^{-2}. To assess the significance of this value, the density of interface charge traps (N_{it}) is an important parameter to estimate. Indeed, these traps, and the associated low frequency noise, are likely to screen the charges provided by the target DNA and can therefore hinder the operation of the biosensor [39]. Therefore, it is essential that the trap density is smaller than the charge density provided by the target DNA. In these devices, the interface quality was quite good, with a density of interface traps of the order of $N_{it} = 4 \times 10^{10}$ cm^{-2}, as estimated from the subthreshold voltage slope (75 mV/dec) and integration on the silicon bandgap. Therefore, even if $|N_{hybrid}|$ was larger than N_{it}, these values remained quite close to each other, which could contribute to the dispersion in the results. Finally, knowing that each strand of target DNA was carrying 19 negative charges (19 nucleotides), the surface density of hybridized DNA density could be estimated to be in the range of 10^{10} cm^{-2}.

6. Conclusion

In this paper a CMOS industry grade low cost process to fabricate SiNWs and SiNRs on wafer scale has been exposed. The 60 nm wide SiNWs reported in this work were fabricated using STL process, were integrated in the back gate transistor configuration and were further functionalized to form DNA biosensors. The SiNW/NR surface was encapsulated with a thin stack of 4 nm SiO_2 and 4.5 nm HfO_2 on which DNA probes were covalently grafted. The efficiency of the bio-functionalization was first assessed by optical experiment thanks to the use of fluorescent DNA targets. Once the process validated, the electrical response of the sensors to single and double stranded DNA was measured. These biosensors allowed detection of DNA hybridization by field effect through the monitoring of transistor threshold voltage (V_{th}) shifts after rinsing and drying. The positive V_{th} shift upon hybridization was in good agreement with the expected supply of negative charges at device surface by target DNA strands suggesting that for SiNWs the dominant mechanism upon drying is the balancing of the negative charge of the DNA target molecules by changes in the concentration of free carriers in the NWs. Experimental observations showed that, due to geometrical effects, only the longest devices were able to detect DNA hybridization electrically. This was attributed to the fact that the window giving access to device surface needs to have a minimum size to allow proper diffusion of the liquids used during biochemical steps and proper DNA probes grafting. Moreover, a statistical study on 33 devices demonstrated that more than 85% of the biosensors were efficient for DNA hybridization detection. The estimated density of hybridized DNA was in the order of 10^{10} cm^{-2}. These promising results pave the way for the fabrication of POC devices, co-integrating SiNW biosensors and CMOS circuitry on the same tier and offering reliable, label-free and fast electrical readout for DNA hybridization detection. The next step is to statistically study the selectivity and sensitivity of such biosensors.

Acknowledgments

This work has been supported by the Nanonets2Sense project fund by the European Horizon 2020 Program under grant agreement 688329. MyFab, the Swedish national research infrastructure for micro and nano fabrication, is acknowledged for their contribution.

Author contribution statement

GJ fabricated the devices, designed the experiments and performed the electrical characterization at the wafer scale. PEH supervised those experiments. ML performed

experiments linked to biosensing. IPP performed confocal microscope observations. ML, CT and VS designed those experiments. MM and PE contributed to methods, analysis and discussion of results. GJ and CT wrote the paper, ML, VS, PE and MM revised it.

Conflict of interest

The authors declare no competing financial interests.

ORCID iDs

Ganesh Jayakumar https://orcid.org/0000-0001-9690-2292
Valérie Stambouli https://orcid.org/0000-0003-0457-4119
Céline Ternon https://orcid.org/0000-0001-8890-4239

References

[1] Serre P, Stambouli V, Weidenhaupt M, Baron T and Ternon C 2015 *Biosens. Bioelectron.* **68** 336
[2] Curreli M, Ishikawa F N, Cote R J and Thompson M E 2008 *IEEE Trans. Nanotechnol.* **7** 651
[3] Yang K, Wang H, Zou K and Zhang X 2006 *Nanotechnology* **17** S276
[4] Balasubramanian K 2010 *Biosens. Bioelectron.* **26** 1195
[5] So H-M, Won K, Kim Y H, Kim B-K, Ryu B H, Na P S, Kim H and Lee J-O 2005 *J. Am. Chem. Soc.* **127** 11906
[6] Gao X P A, Zheng G and Lieber C M 2010 *Nano Lett.* **10** 547
[7] Gao A, Lu N, Wang Y and Li T 2016 *Sci. Rep.* **6** 22554
[8] Gao Z, Agarwal A, Trigg A D, Singh N, Fang C, Tung C H and Buddharaju K D 2007 *TRANSDUCERS 2007—2007 Int. Solid-State Sensors, Actuators and Microsystems Conf.* (Piscataway, NJ: IEEE) pp 2003–6
[9] Wanekaya A K, Chen W, Myung N V and Mulchandani A 2006 *Electroanalysis* **18** 533
[10] Zhang G-J, Huang M J, Luo Z H H, Tay G K I, Lim E-J A, Liu E T and Thomsen J S 2010 *Biosens. Bioelectron.* **26** 365
[11] Chen S 2013 Electronic sensors based on nanostructured field-effect devices *PhD Thesis* Uppsala University
[12] Jayakumar G, Asadollahi A, Hellström P-E, Garidis K and Östling M 2014 *Solid State Electron.* **98** 26
[13] Jayakumar G, Garidis K, Hellstrom P-E and Ostling M 2014 *2014 15th Int. Conf. on Ultimate Integration on Silicon (ULIS)* (Piscataway, NJ: IEEE) pp 109–12
[14] Elfström N, Karlström A E and Linnros J 2008 *Nano Lett.* **8** 945
[15] Knopfmacher O 2011 Sensing with silicon nanowire field-effect transistors *PhD Thesis* University of Basel
[16] Rigante S *et al* 2015 *ACS Nano* **9** 4872
[17] Knopfmacher O, Tarasov A, Fu W, Wipf M, Niesen B, Calame M and Schonenberger C 2010 *Nano Lett.* **10** 2268
[18] Rigante S 2014 High-K dielectric FinFETs on Si-bulk for ionic and biological sensing integrated circuits EPFL *PhD Thesis* (10.5075/epfl-thesis-6134) IEL
[19] Bae T-E, Jang H-J, Yang J-H and Cho W-J 2013 *ACS Appl. Mater. Interfaces* **5** 5214
[20] Star A, Tu E, Niemann J, Gabriel J-C P, Joiner C S and Valcke C 2006 *Proc. Natl Acad. Sci. USA* **103** 921
[21] Knopfmacher O, Keller D, Calame M and Schönenberger C 2009 *Proc. Chem.* **1** 678
[22] Bergveld P 2003 *Sensors Actuators* **88** 1
[23] De A, van Nieuwkasteele J, Carlen E T and van den Berg A 2013 *Analyst* **138** 3221
[24] Joo S and Brown R B 2008 *Chem. Rev.* **108** 638
[25] Chen X, Zhang J, Wang Z, Yan Q and Hui S 2011 *Sensors Actuators* B **156** 631
[26] Dorvel B R, Reddy B, Go J, Duarte Guevara C, Salm E, Alam M A and Bashir R 2012 *ACS Nano* **6** 6150
[27] Lucovsky G 2001 *J. Vac. Sci. Technol.* A **19** 1553
[28] Rigante S, Lattanzio L and Ionescu A M 2011 *Microelectron. Eng.* **88** 1864
[29] Shen S H, Wang I S, Cheng H and Lin C T 2015 *Sensors Actuators* B **218** 303
[30] He G, Zhu L, Sun Z, Wan Q and Zhang L 2011 *Prog. Mater. Sci.* **56** 475
[31] Kirsch P D, Quevedo-Lopez M A, Li H-J, Senzaki Y, Peterson J J, Song S C, Krishnan S A, Moumen N, Barnett J and Bersuker G 2006 *J. Appl. Phys.* **99** 23508
[32] Nair P R and Alam M A 2007 *IEEE Trans. Electron Devices* **54** 3400
[33] F L, B E, A G, R F and Stambouli V 2016 *Nanotechnology* **27** 235501
[34] Squires T M, Messinger R J and Manalis S R 2008 *Nat. Biotechnol.* **26** 417
[35] Kim S J, Jung J, Lee K W, Yoon D H, Jung T S, Dugasani S R, Park S H and Kim H J 2013 *ACS Appl. Mater. Interfaces* **5** 10715
[36] Fu D and Li L-J 2010 *Nano Rev.* **1** 5354
[37] Chu C-J, Yeh C-S, Liao C-K, Tsai L-C, Huang C-M, Lin H-Y, Shyue J-J, Chen Y-T and Chen C-D 2013 *Nano Lett.* **13** 2564
[38] Shaya O, Shaked M, Doron A, Cohen A, Levy I and Rosenwaks Y 2008 *Appl. Phys. Lett.* **93** 43509
[39] Lee J W, Yun W S and Ghibaudo G 2014 *J. Appl. Phys.* **115** 194501